Nanoscale

ROYAL SOCIETY OF CHEMISTRY

PAPER

View Article Online
View Journal | View Issue

Cite this: *Nanoscale*, 2024, **16**, 13457

Assembly of anionic silver nanoclusters with controlled packing structures through site-specific ionic bridges†

Wataru Ishii,[a] Rika Tanaka[b] and Takuya Nakashima *[a]

Received 18th April 2024,
Accepted 11th June 2024

DOI: 10.1039/d4nr01691b

rsc.li/nanoscale

The assembly of metal nanoclusters (NCs) into crystalline lattice structures is of interest in the development of NC-based functional materials. Here we demonstrate that the assembled structures of tri-anionic tetrahedral symmetric $[Ag_{29}(BDT)_{12}]^{3-}$ (Ag_{29} NC, BDT: 1,3-benzenedithiol) NCs are controlled into a polyethylene-like zigzag chain and a "poly-ring-fused-cyclohexane"-like honeycomb arrangement through ionic interactions with alkali metal cations such as K^+ and Cs^+. The site-specific binding of alkali metal ions on the tetrahedrally arranged binding sites of Ag_{29} NCs successfully connects the adjacent NCs into various packing modes. The number and type of bridges between NCs determine the Ag_{29} NC packing structures, which are affected by the solvent species, enabling the transformation of packing modes in the single-crystalline state. The photoluminescence (PL) properties of the crystals responded to the packing modes of the NCs in terms of anisotropy and bridge linkage style inducing a varied degree of relaxation of the excited state depending on the relocation mobility of alkali metal ions in the crystals.

Introduction

Metal nanoclusters (NCs) formed of defined numbers of metal atoms and ligands exhibit structure- and composition-dependent physicochemical properties due to their unique geometrical and electronic structures.[1–5] In the past few decades, efforts to express desired functions for NCs have focused on customizing structural factors such as surface ligands and metal ion species.[6–9] The self-assembly of NCs into crystals has provided an effective means to modulate their intrinsic properties, including optical,[10] electronic,[11] magnetic[12] and spin electronic ones.[13] The controlled-assembly of NCs into crystals has been achieved *via* supramolecular[14–18] approaches and metal organic framework (MOF)-forming strategies.[19–25] The former, driven by intramolecular nonvcovalent interactions, can generate assemblies ranging from simple one-dimensional structures to complex ones such as a double helix. The latter enables the control of hierarchical structures through linker engineering, connecting NC nodes in a site-specific manner. Adjusting the number, length and substituents of N-heteroaromatic linker ligands that coordinate with surface Ag atoms site-specifically facilitated the construction of 1D-to-3D silver cluster-assembled materials, which exhibit temperature-dependent PL properties,[19,20] oxygen sensing properties[21] and gas storage capabilities.[22] In addition to organic ligands, counter ions of NCs could also serve as linkers. Since most NCs are charged to form ionic compounds to fulfill the closed-shell structure in the superatomic orbitals,[26] ionic interactions between intrinsically charged NC bodies and counter ions also play a key role to construct NC-based superstructures.[27,28] For example, silver-based cationic NCs formed multi-dimensional superstructures through ionic linkage by their counter anions such as SbF_6^-, CO_3^{2-}, and $CO_2CF_3^-$.[29–31] The site-specific ionic bonding of counter ions determined the ordering of NCs in the crystals. While ionic interactions are nonspecific and directionless, the size, shape, charge number and coordination number of ionic species and accompanying weak interactions such as hydrogen bonds could also influence the NCs' arrangement.

The $[Ag_{29}(BDT)_{12}(TPP)_4]^{3-}$ (BDT: 1,3-benzenedithiol, TPP: triphenylphosphine) NC (Ag_{29} NC)[32–37] is one of the most studied silver-based luminescent NCs. Its atomically precise structure was clearly disclosed by single crystal X-ray diffraction (SCXRD) analysis,[32] also implying its intrinsically chiral structure.[35] Some recent efforts have focused not only on enhancing the PL performance[34] but also extending the photo-[36] and electronic-[37] functional properties. The Ag_{29} NC

[a]*Department of Chemistry, Graduate School of Science, Osaka Metropolitan University, Sumiyoshi, Osaka 558-8585, Japan.*
E-mail: takuya.nakashima@omu.ac.jp
[b]*X-ray Crystal Analysis Laboratory, Graduate School of Engineering Osaka Metropolitan University, Sumiyoshi, Osaka 558-8585, Japan*

†Electronic supplementary information (ESI) available. CCDC 2076349, 2298858 and 2298942–2298944 for **Ag_{29}-Na**, **Ag_{29}-Cs**, **Ag_{29}-K**, **Ag_{29}-K′** and **Ag_{29}-K″**. For ESI and crystallographic data in CIF or other electronic format see DOI: https://doi.org/10.1039/d4nr01691b

exists as a trianion species to follow the electron count rule of the superatom theory,[26] and its counter cations can be modified by choosing a reductant ($M^+BH_4^-$) or adding a salt. The positions of counter cations (Na^+) were not clearly mentioned in the first report on the single crystal X-ray diffraction (SCXRD) analysis of Ag_{29} NCs.[32] Pradeep and coworkers detected alkali-metal ion bound-Ag_{29} NC species with z value of −2 in their electrospray ionization mass spectrometry (ESI-MS) study. Furthermore, the formation of alkali metal ion-bridged dimers was also identified by ion mobility mass spectrometry (IM MS).[38] The Zhu group reported various types of packing mode in the crystal structures of Ag_{29} NCs with Cs^+.[39,40] Together with oxygen-containing solvent molecules such as DMF, Cs^+ ions linked NCs to form assemblies through Cs^+–π, –O and –S interactions. The assembly dimensions were dependent on the kinds of oxygen-carrying solvent molecules controlling the position of linkage formation.[40] Recently, we found that some sulfur sites ligating two Ag atoms (μ_2-S atoms) of BDT could bind to Na^+ ions or Ag(I)-complexes on the surface of Ag_{29} NCs in a site-specific manner in pyridine.[41,42] The Ag_{29} NC possesses a core–shell structure with a centred icosahedral Ag_{13} superatom surrounded by an exterior shell ($Ag_{16}S_{24}$) composed of two types of building units including four $Ag_3\mu_2$-S_3 crowns and four $Ag_1\mu_3$-S_3 motifs. Both types of building units are arranged in a tetrahedral configuration (Fig. S1†)[32] and the former was involved in the site specific binding of Na^+ ions and Ag(I)-complexes.[40,41] One of the four $Ag_3\mu_2$-S_3 crowns accumulates three Na^+ ions simultaneously using all three μ_2-S sites in the crown, forming an Na_3-triangle incorporating a nitrate anion in its centre (Fig. S2†).[41] Meanwhile, one of the μ_2-S sites in each $Ag_3\mu_2$-S_3 crown was occupied by a bulky Ag(I)complex (Fig. S3†).[42] The binding of Na^+ required light irradiation to activate the S–Na^+ binding whereas the Ag(I) species with the higher affinity to the sulfur atom simultaneously bound to the μ_2-S sites. Although the binding of Na^+ and Ag(I)-complexes was completed in a single-NC,[41,42] the bridging of NCs should occur if cationic species are shared between multiple NCs.

In this study, we demonstrate how the binding of Cs^+ and K^+ counter cations regulates the arrangements of Ag_{29} NCs in their assemblies. The binding sites of these cations, $Ag_3\mu_2$-S_3 crowns, are tetrahedrally arranged on the surface of the Ag_{29} NC in a similar manner to the sp^3-hybrid orbitals of carbon. Given that all four crown sites were used for the bridging of NCs, a diamond-like arrangement of the NCs could be expected. Practically, Cs^+ ions occupied three of the four crown sites bridging NCs to form a wavy honeycomb network. In the case of K^+-mediated assemblies, two crown sites are used for linking NCs, leading to a polyethylene-like zigzag assembly, which further transforms into a honeycomb network with a solvent stimulus. All those structures could be obtained as a consequence of site-specific bridging of NCs with the tetrahedrally arranged connection sites. Photoluminescence (PL) analysis of the crystals suggests that the emission band is indicative of the degree of stabilization in the ligand-to-metal charge transfer (LMCT) state induced by the counter cation translocation in the excited state, which is dependent on the packing modes of the NCs.

Results and discussion

$Ag_{29}(BDT)_{12}(TPP)_4$ NCs were prepared through the reduction of Ag^+ ions using $CsBH_4$ or KBH_4 in the presence of ligands, BDT and TPP. The purified powder of NCs was dispersed in pyridine under ambient light conditions to facilitate the binding of alkali metal ions to the μ_2-S binding sites. Single crystals were obtained in pyridine solutions by vapor diffusion of diethyl ether. While **Ag_{29}-Cs** afforded needle-like crystals, polymorphism was observed for Ag_{29}-K with hexagon and needle-like crystals (**Ag_{29}-K** and **Ag_{29}-K′**, respectively) (Fig. S4†). The impact of alkali metal cations on the packing structures in crystals was examined by SCXRD study. All crystals (**Ag_{29}-Cs**, **Ag_{29}-K** and **Ag_{29}-K′**) have an identical basic composition $M_3[Ag_{29}(BDT)_{12}(TPP)_3(pyridine)_1]$, in which one of the TPP sub-ligands was replaced with a pyridine molecule, and the same space group of $P\bar{1}$ (Fig. S5 and Table S1†). However, different packing modes of the NCs were observed depending on the bridging numbers and positions between NCs with the aid of alkali metal ions.

The employment of Cs^+ ions afforded the quasi-2D-array assembly of Ag_{29} NCs (Fig. 1). One Ag_{29} NC directly anchored 6 Cs^+ ions at the μ_2-S sites and the Cs^+ ions also carry some pyridine or H_2O molecules (Fig. 1a). A pair of Cs^+ ions are shared by two adjacent NCs at each bridging site to form a double linkage. An **Ag_{29}-Cs** unit occupies an apex of a cyclohexane-like wavy hexagon in the wavy honeycomb network of NCs and double linkages are formed at three different crown sites on the same NC linking neighbors upward and downward alternately (Fig. 1b and e). The average interNC distance between neighboring NCs (between the kernel-center Ag atoms) is about 19 Å (Fig. 1b). The wavy honeycomb network extends along the *bc* plane, stacking in layers with the formation of one-dimensional channels with a size of 5.0 × 10 Å along the *a*-axis (Fig. 1d and g). It should be noted that one tetravalent Ag site with the Ag_1S_3 motif was bound by a pyridine molecule along the *a*-axis and the other sites were coordinated by TPP ligands sticking out toward the center of the channel (Fig. S6†). While no Cs^+ bridging linkage is observed in the interlayer of the honeycomb networks, the average distance for the interlayer spacing is estimated to be 19 Å (Fig. 1e). The direct attachment of the Cs^+ ions to the μ_2-S sites of the Ag_3S_3 crowns triggers the self-assembly of the Ag_{29} NCs into a highly symmetric honeycomb network in the crystalline cell. Zhu and co-workers also reported Cs^+-mediated assembly of Ag_{29} NCs.[39,40] Cs^+ ions assembled Ag_{29} NCs into a 1D-linear chain, 2D-network and 3D-superstructure primarily through interactions with the aromatic ring of BDT and with oxygen carrying solvent molecules such as DMF, NMP and tetramethylene sulfone.[40] In the present study, the photoirradiation conditions in a coordinating solvent activate the Ag–S bonds with the aid of charge transfer to oxygen, facilitating the bond dis-

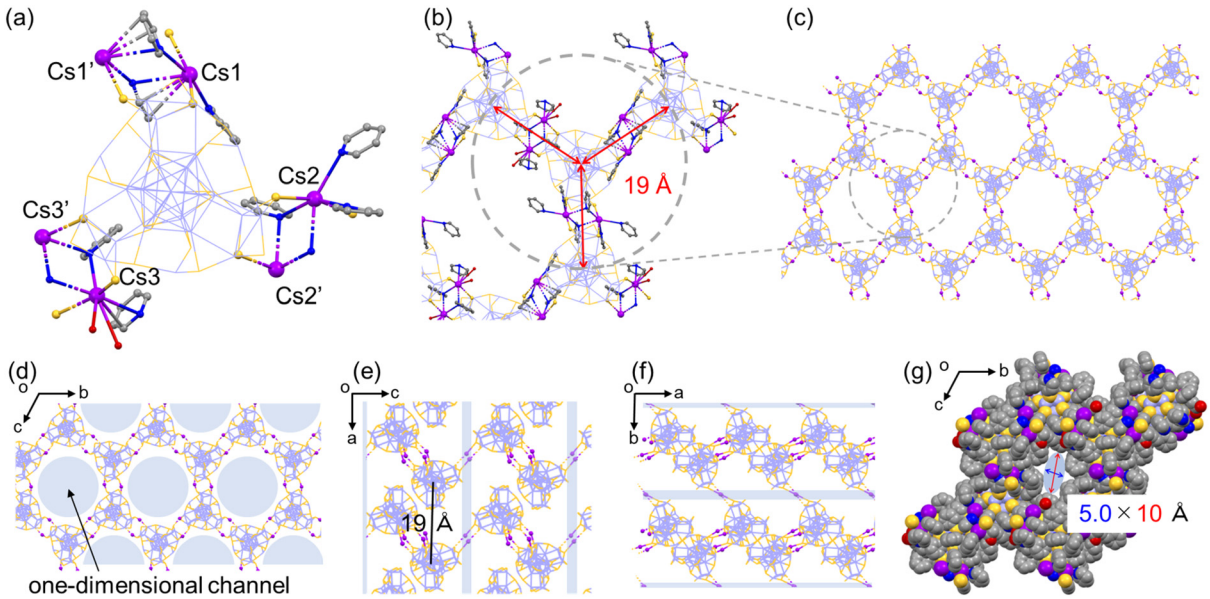

Fig. 1 (a) Unit structure of **Ag_{29}-Cs**. (b) Packing structure of **Ag_{29}-Cs** highlighting the bridging style between adjacent NCs. (c) Wavy honeycomb network composed of **Ag_{29}-Cs**. Packing structure of **Ag_{29}-Cs** from the (d) *a*-axis, (e) *b*-axis, (f) *c*-axis. (g) Spacefill packing structure of **Ag_{29}-Cs** without H atoms. Color code: violet, Ag; yellow, S; purple, Cs; blue, N; red, O. The solvents and H, C, N and P atoms in NC ligands are omitted for clarity except in (g).

sociation to form S^- sites with stabilizing Ag^+ sites in the presence of pyridine molecules.[41] While the transiently dissociated Ag–S bonds appear to be regenerated quickly in most media, the metal coordinating capability of pyridine facilitated the transient bond cleavage. The transiently formed S^- sites bound the Cs^+ counter cations, thus forming μ_2S–Cs^+–μ_2S bridges in a site specific manner.

A unique honeycomb assembly of Ag_{29} NCs was also observed in the hexagonal crystal of **Ag_{29}-K**, where the interNC bridging mode was a bit different from that of **Ag_{29}-Cs** (Fig. 2). Three crown sites were used for the binding of K^+ ions in a similar manner to **Ag_{29}-Cs**. The number of K^+ ions which anchored directly to the surface of the same NC is five, while the ratio between Ag_{29} NCs and K^+ ions is 1 : 3, balancing the

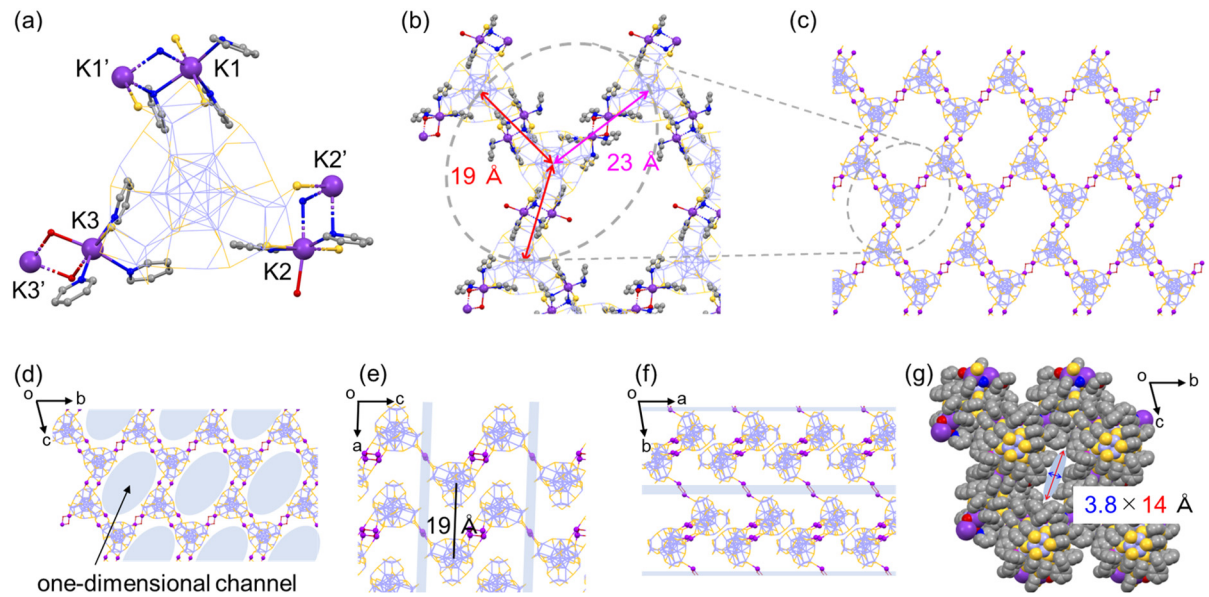

Fig. 2 (a) Unit structure of **Ag_{29}-K**. (b) Packing structure of **Ag_{29}-K** highlighting the bridging style between adjacent NCs. (c) distorted quasi-2D honeycomb structure composed of **Ag_{29}-K**. Packing structure of **Ag_{29}-K** from the (d) *a*-axis, (e) *b*-axis, (f) *c*-axis. (g) Spacefill packing structure of **Ag_{29}-K** without H atoms. Color code: violet, Ag; yellow, S; purple, K; blue, N; red, O. The solvents and H, C, N and P atoms in NC ligands are omitted for clarity except in (g).

net charge. In addition to the formation of double linkages at two bridging sites (K1–K1′ and K2–K2′) in a similar manner to those of **Ag_{29}-Cs**, the remaining bridging site forms a single linkage of K3–$(H_2O)_2$–K3′ with a larger interNC distance (Fig. 2a and b). The existence of two types of NC-bridging styles results in different interNC distances (19 Å and 23 Å), forming the distorted wavy honeycomb structure in the crystal packing (Fig. 2b and c). The distorted honeycomb network extends along the *bc* plane, stacking along the *a*-axis with the interlayer distance of 19 Å (Fig. 2e) to form the one-dimensional channel with the size of 3.8 × 14 Å (Fig. 2g). Three TPP molecules among four Ag_1S_3 binding motifs were also coordinated from the center of the channel (Fig. S7†).

Another crystal of Ag_{29}-K with the needle shape (**Ag_{29}-K′**) contains a polyethylene-like zigzag chain arrangement of NCs extended along the *c*-axis (Fig. 3). While two of three K^+ ions per single NC could be identified, two crown sites were bound to four K^+ ions at the μ_2-S sites on the surface of the Ag_{29} NC (Fig. 3a). The double linkage style at two sites arranged the NCs in a zig-zag manner (Fig. 3b and c). The interNC distance between two linking NCs is about 19 Å (Fig. 3b). The distance between two adjacent chains is also 19 Å (Fig. 3e).

Considering that even with the employment of the same alkali metal cation family the aforementioned assembled structural variation was induced in the same solvent system (pyridine/diethylether), the solvent-stimuli should also impact the crystal packing structure. To the best of our knowledge, structural isomerization of NCs in a single crystal as a result of solvent stimuli has rarely been reported.[20,43–45] Only one example has demonstrated NC-based supramolecular polymorphism.[45] Interestingly, we found that the **Ag_{29}-K′** crystal exhibited a structural transformation after being immersed in toluene for several days (Fig. 4, **Ag_{29}-K″**). As shown in Fig. S8,† the thin needle-like crystals curved after toluene soaking suggesting certain changes in the NC structure and/or their packing mode. Since those curved thin crystals were not suitable for SCXRD study, a larger crystal was subjected to measurement. The packing mode of the NCs indeed changed. The number of bridging sites with the double linkage increased from two to three. In short, the polyethylene-like packing transformed into the regular wavy honeycomb network similar to that of **Ag_{29}-Cs** (Fig. S9†). As the ion radius decreased compared to Cs^+, a slightly smaller channel size was observed (5.0 × 9.4 Å, Fig. 4g). In toluene with a lower dielectric constant, the presence of solvated or unbound K^+ ions should be less possible unlike in pyridine solution, and all K^+ ions were employed for the bridge formation. Meanwhile, structural transformation could not be observed for the **Ag_{29}-K** (distorted honeycomb) crystal soaked in toluene for several days probably due to the strong binding of H_2O molecules in the K3–$(H_2O)_2$–K3′ bridge and the lower miscibility of water with toluene.

Scheme 1 summarizes the relationship between the alkali cation species and packing structure. When Na^+ ions with a smaller ionic radius (1.0 Å) serve as counter cations, they can accumulate on an identical $Ag_3\mu_2$-S_3 crown site with binding to all three sulfur atoms.[41] Meanwhile, the larger K^+ (1.4 Å) and Cs^+ (1.7 Å) could occupy two sulfurs at most while bridging different Ag_{29} NCs. The more hydrophilic K^+ ion may carry water molecules as a solvated molecule to give **Ag_{29}-K**. The stronger interaction of K^+ with solvent molecules such as pyridine and dissolved water molecules than with the sulfur site may result in an uninvolved K^+ ion for **Ag_{29}-K′**, while the

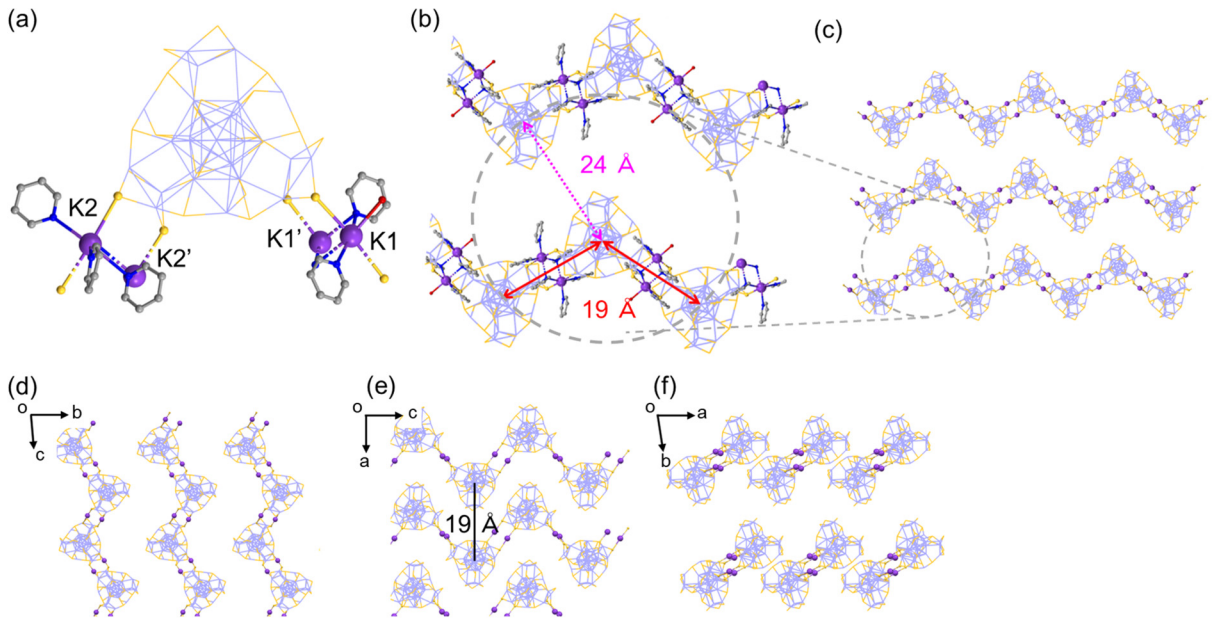

Fig. 3 (a) Unit structure of **Ag_{29}-K′**. (b) Packing structure of **Ag_{29}-K′** highlighting the bridging style between adjacent NCs. (c) Polyethylene-like 1D chain structure composed of **Ag_{29}-K′**. Packing structure of **Ag_{29}-K′** from the (d) *a*-axis, (e) *b*-axis, (f) *c*-axis. Color code: violet, Ag; yellow, S; purple, K; blue, N; red, O. The solvents and H, C, N and P atoms in NC ligands are omitted for clarity.

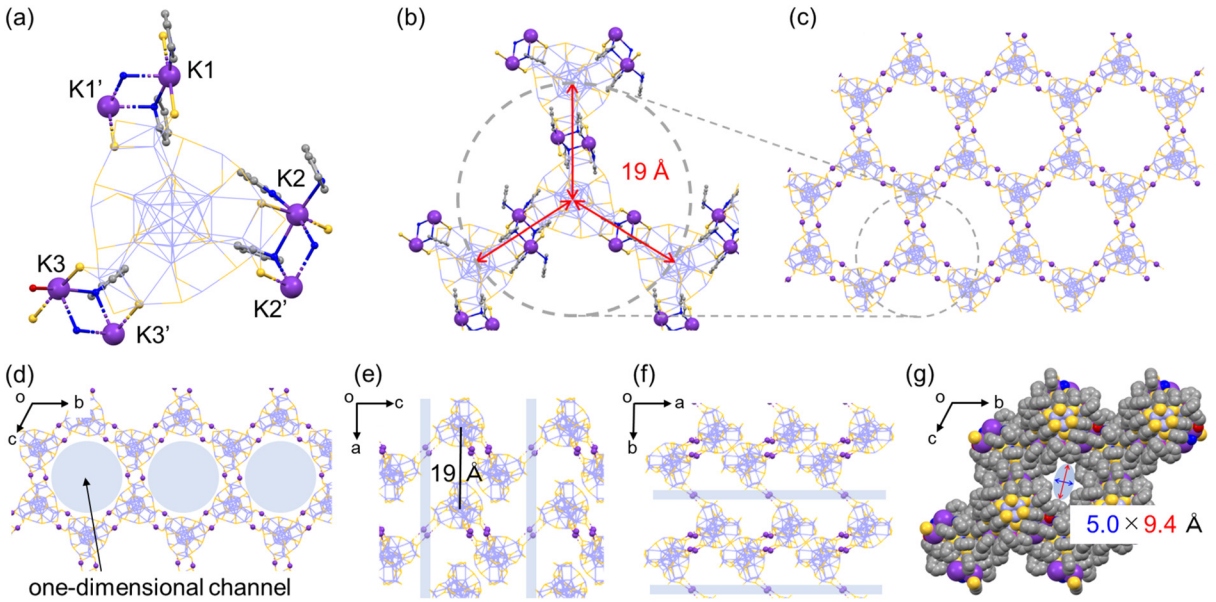

Fig. 4 (a) Unit structure of **Ag_{29}-K″**. (b) Packing structure of **Ag_{29}-K″** highlighting the bridging style between adjacent NCs. (c) Quasi-2D honeycomb structure composed of **Ag_{29}-K″**. Packing structure of **Ag_{29}-K″** from the (d) *a*-axis, (e) *b*-axis, (f) *c*-axis. (g) Spacefill packing structure of **Ag_{29}-K″** without H atoms. Color code: violet, Ag; yellow, S; purple, K; blue, N; red, O. The solvents and H, C, N and P atoms in NC ligands are omitted for clarity except in (g).

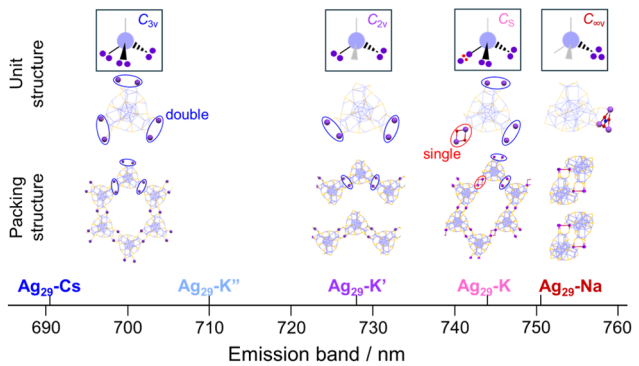

Scheme 1 Relationships between the crystal packing structures and their emission bands.

exposure to less polar toluene relocated the unbound K^+ to the $Ag_3\mu_2$-S_3 crown binding site in **Ag_{29}-K″**.

In order to obtain an insight into the relationship between structure and PL properties, we measured PL spectra in solution and crystal states. In pyridine solutions, emission bands were observed at 770 nm with PLQYs of 30–40% and PL lifetimes around 10 μs for all samples regardless of the counter cationic species (Fig. S10, S11 and Table S3†). The excitation spectra almost reproduced the absorption spectra with a peak at 445 nm and a shoulder around at 500 nm. The PL origin for the Ag_{29}-based NCs has been attributed to the LMCT state with a triplet character.[32,46,47] Previously, we proposed that the cationic metal ions bound to the peripheral region of Ag_{29} NCs play a role in stabilizing the LMCT based excited state, resulting in a shift of the emission band from 680 nm to 770 nm (in the near infrared (NIR) region) as well as an increase in the PL lifetime in solution.[42] The transient absorption study suggested the relocation of surface-bound metal ions or the compaction of the NC-shell in the time scale of 300 ps to stabilize the more negatively charged core in the LMCT state. In the crystalline states, such translocation is potentially restricted depending on the packing structure of the NCs.

In contrast to the solution state, these crystals exhibited different emission bands at 692 (**Ag_{29}-Cs**), 744 (**Ag_{29}-K**), 728 (**Ag_{29}-K′**), 710 (**Ag_{29}-K″**) and 751 nm (**Ag_{29}-Na**), respectively (Fig. 5). The crystals exhibited moderate photostability, where extended photoirradiation (~ a few dozen minutes) in air led to the photodegradation. Different packing modes may lead to the structural variation of the NCs[20] including the core Ag_{13} symmetry, resulting in the different electronic structures affecting the PL properties. However, little differences in the

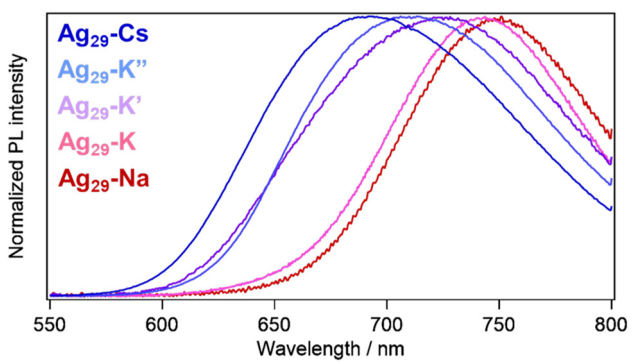

Fig. 5 PL spectra of **Ag_{29}-Cs**, **K**, **K′**, **K″** and **Na** crystals.

NC-unit structures including core and shell ones were observed for these crystals (Fig. S11 and Table S2†). The varied PL peak positions could be explained in terms of different packing modes of the NCs including the symmetry and bonding styles (Scheme 1). The binding of each alkali metal cation with different numbers and binding styles reduced the symmetry of the T_d Ag_{29} NC unit to C_{3v} (in **Ag_{29}-Cs** and **Ag_{29}-K″**), C_{2v} (in **Ag_{29}-K′**), C_S (in **Ag_{29}-K**) and $C_{\infty v}$ (in **Ag_{29}-Na**). The lower symmetric unit structures increased the anisotropy of the packing structure, enabling a particular ionic motion or relocation that induced the NIR PL activation (**Ag_{29}-Na** and **Ag_{29}-K**). For the case of **Ag_{29}-Na**, the binding of cations was completed in a single NC, ensuring the mobility of Na^+. In addition to the lower symmetry, one of the bridging styles of NCs includes a single linkage for **Ag_{29}-K**, which also works better for the excited state relocation of K^+. Conversely, the highly symmetric and rigid honeycomb quasi-2D structure formed by the double linkage styles would suppress the translocation of metal ions, resulting in less red-shifted PL compared to the pristine PL in DMF solution[32,34] (**Ag_{29}-Cs** and **Ag_{29}-K″**). To partly support this explanation, we compared the PL lifetimes for three different crystals, **Ag_{29}-K**, **-K′** and **-K″**. The presence of a fast component (~1.4 μs) for **Ag_{29}-K** suggests the contribution of more flexible single bonds (K3–$(H_2O)_2$–K3′) to the non-radiative decay. However, the average PL lifetime of **Ag_{29}-K** (9.37 μs) was apparently longer than those of **Ag_{29}-K′** (3.70 μs) and **Ag_{29}-K″** (4.33 μs), suggesting the excited state transition to a long-lived state for **Ag_{29}-K**.

Despite a noticeable change in the crystal PL properties, a slight difference was observed in the absorption spectra (Fig. S14†). Each crystal gave a similar absorption spectrum with a peak at 450 nm and a shoulder at around 530 nm. Since the electronic transitions upon light absorption of Ag_{29} NCs occur predominantly between the superatomic P–D orbitals in the Ag_{13} core,[35] the binding of alkali metal cations and the neighbouring NCs had less of an effect on the absorption spectra compared to the PL spectral change.

Conclusion

In conclusion, we have demonstrated that Ag_{29} NCs adopt assembled structures depending on the counter cation species. The tetrahedrally arranged Ag_3S_3 crowns with μ_2-S species in the exterior shell of the Ag_{29} NCs served as bridging sites to connect NCs through the binding of Cs^+ and K^+. The packing modes of the NCs were dependent on the bridging site number and style such as single- and double linkages. Interestingly, the solvent stimulus induced the increase of the number of double linkages, transforming the polyethylene like 1D assembly (**Ag_{29}-K′**) to the quasi-2D wavy honeycomb one (**Ag_{29}-K″**). The diverse PL bands observed in the single crystals could be explained by the packing structure of the NCs, in which the mobility of cations should be dependent on the symmetry and connection nature in the NC arrangement. Given that numerous thiolate-protected NCs carry some negative charge,[48,49] the site-specific ionic bond formation strategy is expected to foster the creation of diverse ordered NC superstructures. The combination of selecting counter cation species and controlling the number of linkers through metal atom doping[50–52] could reveal further potential for functionalizing NC superstructures.

Author contributions

W. I. and T. N. co-wrote the manuscript. W. I. performed most of experimental work including sample preparation and spectroscopic study. R. T. conducted the SCXRD measurement and analysis. T. N. supervised the entire project. All authors commented on and agreed on the manuscript.

Conflicts of interest

The authors declare no competing financial interests.

Acknowledgements

This work was financially supported by JST CREST (Grant Number: JPMJCR20B2), JSPS KAKENHI grant numbers 23H01938 for Scientific Research (B) and JP22H05134 (TN) for Transformative Research Areas (A) “Revolution of Chiral Materials Science using Helical Light.

References

1 R. Jin, C. Zeng, M. Zhou and Y. Chen, *Chem. Rev.*, 2016, **116**, 10346–10413.
2 I. Chakraborty and T. Pradeep, *Chem. Rev.*, 2017, **117**, 8208–8271.
3 S. Takano and T. Tsukuda, *J. Am. Chem. Soc.*, 2021, **143**, 1683–1698.
4 H. Hirai, S. Ito, S. Takano, K. Koyasu and T. Tsukuda, *Chem. Sci.*, 2020, **11**, 12233–12248.
5 X. Kang and M. Zhu, *Chem. Soc. Rev.*, 2019, **48**, 2422–2457.
6 X. Kang, Y. Li, M. Zhu and R. Jin, *Chem. Soc. Rev.*, 2020, **49**, 6443–6514.
7 X. Zou, X. Kang and M. Zhu, *Chem. Soc. Rev.*, 2023, **52**, 5892–5967.
8 J. Yan, B. K. Teo and N. F. Zheng, *Acc. Chem. Res.*, 2018, **51**, 3084–3093.
9 B. Zhang, J. Chen, Y. Cao, O. J. H. Chai and J. Xie, *Small*, 2021, **17**, e2004381.
10 Z. Wu, Y. Du, J. Liu, Q. Yao, T. Chen, Y. Cao, H. Zhang and J. Xie, *Angew. Chem., Int. Ed.*, 2019, **58**, 8139–8144.
11 P. Yuan, R. Zhang, E. Selenius, P. Ruan, Y. Yao, Y. Zhou, S. Malola, H. Häkinen, B. K. Teo, Y. Cao and N. Zheng, *Nat. Commun.*, 2020, **11**, 2229.

12 M. De Nardi, S. Antonello, D.-E. Jiang, F. Pan, K. Rissanen, M. Ruzzi, A. Venzo, A. Zoleo and F. Maran, *ACS Nano*, 2014, **8**, 8505–8512.
13 N. Xia, J. Xing, D. Peng, S. Ji, J. Zha, N. Yan, Y. Su, X. Jiang, Z. Zeng, J. Zhao and Z. Wu, *Nat. Commun.*, 2022, **13**, 5934.
14 Y. Li, M. Zhou, Y. Song, T. Higaki, H. Wang and R. Jin, *Nature*, 2021, **594**, 380–384.
15 H. Li, P. Wang, C. Zhu, W. Zhang, M. Zhou, S. Zhang, C. F. Zhang, Y. P. Yun, X. Kang, Y. Pei and M. Z. Zhu, *J. Am. Chem. Soc.*, 2022, **144**, 23205–23213.
16 G. L. Dong, Z. H. Pan, B. L. Han, Y. W. Tao, X. Chen, G. G. Luo, P. P. Sun, C. F. Sun and D. Sun, *Angew. Chem., Int. Ed.*, 2023, **62**, e202302595.
17 J.-H. Huang, Z.-Y. Wang, S.-Q. Zang and T. C. W. Mak, *ACS Cent. Sci.*, 2020, **6**, 1971–1976.
18 S. Hossain, Y. Imai, Y. Motohashi, Z. Chen, D. Suzuki, T. Suzuki, Y. Kataoka, M. Hirata, T. Ono, W. Kurashige, T. Kawawaki, T. Yamamoto and Y. Negishi, *Mater. Horiz.*, 2020, **7**, 796–803.
19 Z.-Y. Wang, M.-Q. Wang, Y.-L. Li, P. Luo, T.-T. Jia, R.-W. Huang, S.-Q. Zang and T. C. W. Mak, *J. Am. Chem. Soc.*, 2018, **140**, 1069–1076.
20 R.-W. Huang, X.-Y. Dong, B.-J. Yan, X.-S. Wei, D.-H. Wei, S.-Q. Zang and T. C. W. Mak, *Angew. Chem., Int. Ed.*, 2018, **57**, 8560–8566.
21 R.-W. Huang, Y.-S. Wei, X.-Y. Dong, X.-H. Wu, C.-X. Du, S.-Q. Zang and T. C. W. Mak, *Nat. Chem.*, 2017, **9**, 689–697.
22 X.-Y. Dong, Y. Si, J.-S. Yang, C. Zhang, Z. Han, P. Luo, Z.-Y. Wang, S.-Q. Zang and T. C. W. Mak, *Nat. Commun.*, 2020, **11**, 3678.
23 M. Cao, R. Pang, Q.-Y. Wang, Z. Han, Z.-Y. Wang, X.-Y. Dong, S.-F. Li, S.-Q. Zang and T. C. W. Mak, *J. Am. Chem. Soc.*, 2019, **141**, 14505–14509.
24 M. J. Alhilaly, R.-W. Huang, R. Naphade, B. Alamer, M. N. Hedhili, A.-H. Emwas, P. Maity, J. Yin, A. Shkurenko, O. F. Mohammed, M. Eddaoudi and O. M. Bakr, *J. Am. Chem. Soc.*, 2019, **141**, 9585–9592.
25 M. H. Zhao, S. Huang, Q. Fu, W. F. Li, R. Guo, Q. X. Yao, F. L. Wang, P. Cui, C. H. Tung and D. Sun, *Angew. Chem., Int. Ed.*, 2020, **59**, 20031–20036.
26 M. Walter, J. Akola, O. Lopez-Acevedo, P. D. Jadzinsky, G. Calero, C. J. Ackerson, R. L. Whetten, H. Grönbeck and H. Häkkinen, *Proc. Natl. Acad. Sci. U. S. A.*, 2008, **105**, 9157–9162.
27 Q. Yao, Y. Yu, X. Yuan, Y. Yu, D. Zhao, J. Xie and J. Y. Lee, *Angew. Chem., Int. Ed.*, 2015, **54**, 184–189.
28 Q. Yao, L. Liu, S. Malola, M. Ge, H. Xu, Z. Wu, T. Chen, Y. Cao, M. F. Matus, A. Pihlajamäki, Y. Han, H. Häkkinen and J. Xie, *Nat. Chem.*, 2023, **15**, 230–239.
29 S. Chen, W. Du, C. Qin, D. Liu, L. Tang, Y. Liu, S. Wang and M. Zhu, *Angew. Chem., Int. Ed.*, 2020, **59**, 7542–7547.
30 Z. Wang, X. Y. Li, L. W. Liu, S. Q. Yu, Z. Y. Feng, C. H. Tung and D. Sun, *Chem. – Eur. J.*, 2016, **22**, 6830–6836.
31 Z. Qin, Z. Li, S. Sharma, Y. Peng, R. Jin and G. Li, *Research*, 2022, **2022**, 0018.
32 L. G. AbdulHalim, M. S. Bootharaju, Q. Tang, S. Del Gobbo, R. G. AbdulHalim, M. Eddaoudi, D. E. Jiang and O. M. Bakr, *J. Am. Chem. Soc.*, 2015, **137**, 11970–11975.
33 A. Nag, P. Chakraborty, M. Bodiuzzaman, T. Ahuja, S. Antharjanam and T. Pradeep, *Nanoscale*, 2018, **10**, 9851–9855.
34 X. Kang, S. Wang and M. Zhu, *Chem. Sci.*, 2018, **9**, 3062–3068.
35 H. Yoshida, M. Ehara, U. D. Priyakumar, T. Kawai and T. Nakashima, *Chem. Sci.*, 2020, **11**, 2394–2400.
36 J.-Y. Wang, Y.-K. Li, X. Jing, P. Luo, X.-Y. Dong and S.-Q. Zang, *ACS Mater. Lett.*, 2022, **4**, 960–966.
37 H. Shen, Q. Zhu, J. Xu, K. Ni, X. Wei, Y. Du, S. Gao, X. Kang and M. Zhu, *Nanoscale*, 2023, **15**, 14941–14948.
38 P. Chakraborty, A. Baksi, S. K. Mudedla, A. Nag, G. Paramasivam, V. Subramanian and T. Pradeep, *Phys. Chem. Chem. Phys.*, 2018, **20**, 7593–7603.
39 X. Wei, X. Kang, Q. Yuan, C. Qin, S. Jin, S. Wang and M. Zhu, *Chem. Mater.*, 2019, **31**, 4945–4952.
40 X. Wei, X. Kang, Z. Zuo, F. Song, S. Wang and M. Zhu, *Natl. Sci. Rev.*, 2021, **8**, nwaa077.
41 W. Ishii, S. Katao, Y. Nishikawa, Y. Okajima, A. Hatori, M. Ehara, T. Kawai and T. Nakashima, *Chem. Commun.*, 2021, **57**, 6483–6486.
42 W. Ishii, Y. Okayasu, Y. Kobayashi, R. Tanaka, S. Katao, Y. Nishikawa, Y. Okajima, T. Kawai and T. Nakashima, *J. Am. Chem. Soc.*, 2023, **145**, 11236–11244.
43 S. Li, Z.-Y. Wang, G.-G. Gao, B. Li, P. Luo, Y.-J. Kong, H. Liu and S.-Q. Zang, *Angew. Chem., Int. Ed.*, 2018, **57**, 12775–12779.
44 Z. Han, Y. Si, X.-Y. Dong, J.-H. Hu, C. Zhang, X.-H. Zhao, J.-W. Yuan, Y. Wang and S.-Q. Zang, *J. Am. Chem. Soc.*, 2023, **145**, 6166–6176.
45 K. Sheng, Z. Wang, L. Li, Z.-Y. Gao, C.-H. Tung and D. Sun, *J. Am. Chem. Soc.*, 2023, **145**, 10595–10603.
46 Y. Zeng, S. Havenridge, M. Gharib, A. Baksi, K. L. D. M. Weerawardene, A. R. Ziefuß, C. Strelow, C. Rehbock, A. Mews, S. Barcikowski, M. M. Kappes, W. J. Parak, C. M. Aikens and I. Chakraborty, *J. Am. Chem. Soc.*, 2021, **143**, 9405–9414.
47 E. Khatun, A. Ghosh, P. Chakraborty, P. Singh, M. Bodiuzzaman, P. Ganesan, G. Nataranjan, J. Ghosh and S. K. Pal, *Nanoscale*, 2018, **10**, 20033–20042.
48 X. Kang, H. Chong and M. Zhu, *Nanoscale*, 2018, **10**, 10758–10834.
49 Q. Yao, P. Chen, Y. Yuan and J. Xie, *Acc. Chem. Res.*, 2018, **51**, 1338–1348.
50 H. Hirai, S. Takano, T. Nakashima, T. Iwasa, T. Taketsugu and T. Tsukuda, *Angew. Chem., Int. Ed.*, 2022, **61**, e202207290.
51 H. Yi, S. M. Han, S. Song, M. Kim, E. Sim and D. Lee, *Angew. Chem., Int. Ed.*, 2021, **60**, 22293–22300.
52 S. Takano, H. Hirai, T. Nakashima, T. Iwasa, T. Taketsugu and T. Tsukuda, *J. Am. Chem. Soc.*, 2021, **143**, 10560–10564.